PAPER

Check for updates

Low-molecular-weight hyaluronic acid prepared through photoelectric-Fenton reaction protects Caco-2 cells from oxidative damage by regulating metabolites

Jiayi Yan, Youxian Zhou, Chen Song, Yunning Yang, Fanhua Kong, Jingfeng Yang and Shuang Song (ID) *

Hyaluronic acid (HA), which has been extensively used in medicine, cosmetics and food, possesses numerous bioactivities varying with its molecular weight. In the present study, a photoelectric-Fenton depolymerization method was established to prepare low-molecular-weight HA whose antioxidant activity was evaluated in Caco-2 cells through metabonomics analysis. The depolymerization products were monitored by high-performance gel permeation chromatography, thin-layer chromatography, infrared spectra, and nuclear magnetic resonance, and the results suggest 8 mM Fe^{2+} and 0.5% H_2O_2 as the optimal conditions with which 2 low-molecular-weight HA samples, DHA1 and DHA2 with relative molecular weights of 6.7 kDa and 1.6 kDa were obtained after 10 min and 25 min, respectively, in the photoelectric-Fenton system. Moreover, a comparison of HA and its depolymerization products showed minimal disruption of HA's structural units by photoelectric-Fenton reaction. In addition, metabolite analysis by LC-MS/MS revealed that both HA and DHA2 could alleviate cellular oxidative damage through modulating the arginine and proline metabolic pathways by upregulating the content of hydroxyproline and downregulating the levels of L-proline, creatinine, spermidine, L-glutamic acid, and acetyl-CoA. Notably, DHA2 exhibited superior effects compared to original HA. The study indicate that the photoelectric-Fenton degradation process holds great potential to prepare low-molecular-weight HA which possessed better protective capability against oxidative damage.

Sustainability spotlight

This study pioneers a green photoelectro-Fenton (PEF) catalytic system (8 mM Fe2+/0.5% H_2O_2) for rapid, energy-efficient depolymerization of hyaluronic acid (HA) into low-molecular-weight fragments (6.7 kDa in 10 min; 1.6 kDa in 25 min) with preserved bioactivity. The PEF process leverages synergistic photo-electro catalysis to enhance ˙OH generation, minimizing reagent consumption and reaction time compared to conventional methods. The resulting 1.6 kDa HA (DHA2) exhibits superior antioxidant effects in Caco-2 cells by modulating arginine/proline metabolism. This work advances SDG 9 (sustainable industrialization) and SDG 12 (green chemistry) by offering a scalable, eco-friendly strategy to produce high-value bioactive HA derivatives, with potential applications in medicine and food.

1. Introduction

Hyaluronic acid (HA) is a naturally occurring glycosaminoglycan widely distributed in the extracellular matrix of vertebrate tissues, including skin, connective tissue, and synovial fluid. It is composed of repeating disaccharide units of glucuronic acid (GlcA) and *N*-acetylglucosamine (GlcNAc).[1] HA plays crucial roles in maintaining tissue hydration, joint lubrication, and cell migration and proliferation.[2] The biological activities of HA are closely related to its molecular weight, with high-molecular-weight HA (HMW-HA) and low-molecular-weight HA (LMW-HA) exhibiting distinct physiological functions.[3]

High-molecular-weight HA (HMW-HA, >500 kDa) is known for its anti-inflammatory and anti-angiogenic properties. Specifically, HMW-HA can suppress the production of pro-inflammatory cytokines, such as TNF-α and IL-1β, and inhibit the formation of new blood vessels, making it beneficial in conditions like arthritis and cancer.[4,5] In contrast, low-molecular-weight HA (LMW-HA <50 kDa) and HA oligosaccharides (1–10 kDa) demonstrate pro-angiogenic, pro-

SKL of Marine Food Processing & Safety Control, National Engineering Research Center of Seafood, Collaborative Innovation Center of Seafood Deep Processing, National & Local Joint Engineering Laboratory for Marine Bioactive Polysaccharide Development and Application, Liaoning Key Laboratory of Food Nutrition and Health, School of Food Science and Technology, Dalian Polytechnic University, Dalian 116034, China. E-mail: songs1008@163.com

inflammatory, and wound-healing effects. LMW-HA can stimulate the production of growth factors, such as VEGF and FGF-2, promoting angiogenesis and tissue repair, which are crucial for wound healing and regenerative medicine.[6]

In nature, HA is synthesized by hyaluronan synthases and degraded by hyaluronidases and reactive oxygen species (ROS) within the body.[7] However, the natural degradation process is often slow and inefficient for producing HA with specific molecular weights required for various biomedical applications.[8] Consequently, there is a growing interest in developing efficient methods to produce LMW-HA and HA oligosaccharides with targeted molecular weights for use in pharmaceuticals, cosmetics, and food industries.[9,10]

Currently, HA degradation is primarily achieved through chemical, enzymatic, and physical methods.[11] Enzymatic degradation, while specific and mild, is limited by the high cost of enzymes and the difficulty in controlling the degradation process to obtain HA with precise molecular weights.[12] Chemical degradation methods, such as acid hydrolysis, often lack specificity and can lead to undesirable by-products.[13,14] Physical methods, including ultrasonic and thermal degradation, are energy-intensive and may result in inconsistent product quality. Therefore, there is a need for more efficient and controllable degradation techniques to produce LMW-HA with well-defined molecular weights.[15]

Photoelectrocatalysis (PEC) is an advanced oxidation process that combines the advantages of photocatalysis and electrochemical reactions to generate highly reactive species, such as hydroxyl radicals ($^{\bullet}OH$), which can effectively degrade organic compounds.[16,17] In PEC, a semiconductor material, such as TiO_2, is irradiated with light energy exceeding its bandgap, generating electron–hole pairs. The photogenerated electrons (e^-) migrate to the cathode, while the holes (h^+) remain at the anode, prolonging the lifetime of the reactive species and enhancing the degradation efficiency.[18] The Fenton reaction, which involves the generation of $^{\bullet}OH$ radicals through the reaction of Fe^{2+} with H_2O_2, is another powerful oxidation process widely used in wastewater treatment and organic pollutant degradation.[19] The combination of PEC and Fenton reactions, known as the photoelectric-Fenton process, has shown great potential in degrading complex organic molecules due to its high efficiency and ability to generate a large number of reactive species.[20,21]

The photoelectric-Fenton process offers several advantages over traditional degradation methods, including faster reaction rates, lower energy consumption, and the ability to produce LMW-HA with precise molecular weights.[22] This study aims to develop an efficient photoelectric-Fenton catalytic degradation method for HA, optimize the reaction conditions, and characterize the degradation products.[23] Additionally, the protective effects of HA and its degradation products against oxidative damage in intestinal epithelial cells will be investigated using a Caco-2 cell model. The Caco-2 cell line, a human colon adenocarcinoma cell line, is a well-established *in vitro* model of the human intestinal epithelium. It is widely used in nutrient absorption, drug transport, and gut barrier function studies due to its ability to spontaneously differentiate into enterocyte-like cells that form tight junctions and express brush border enzymes.[24] As HA finds significant applications in the food and oral pharmaceutical industries, evaluating its effects on intestinal epithelial cells is highly relevant for assessing its potential bioavailability, functional efficacy in nutraceuticals, and therapeutic benefits for gastrointestinal health, such as mitigating inflammatory bowel diseases (IBD) where oxidative stress plays a key role.[25] The use of this model provides critical preliminary data on the applicability of LMW-HA for developing functional foods aimed at gut health and oral formulations for biomedical applications.[26] By leveraging the synergistic effects of photoelectrocatalysis and Fenton reactions, this study seeks to provide a novel and efficient approach for producing LMW-HA with enhanced bioactivity for various applications[16,26]

In summary, while HA can be naturally synthesized and degraded *in vivo*, the development of advanced degradation techniques, such as the photoelectric-Fenton process, is essential for producing LMW-HA with specific molecular weights for industrial and biomedical applications. This study not only addresses the limitations of existing degradation methods but also explores the potential of LMW-HA in mitigating oxidative damage, thereby contributing to the growing body of knowledge on the functional properties and applications of HA. A schematic diagram of the photoelectric-Fenton reaction system used for HA depolymerization is illustrated in Fig. 1.

2. Materials and methods

2.1. Materials

Hyaluronic acid was sourced from McLean Biochemical Technology Co. (Shanghai). TiO_2 nanoparticles (25 nm) were from Evonik Degussa (Frankfurt). Dextran standards were from Sigma-Aldrich (St. Louis). Chromatography-grade acetonitrile and methanol were purchased from Spectrum Chemical (Shanghai). Caco-2 cells were obtained from the Chinese Academy of Sciences (Shanghai). Culture medium was provided by Thermo Fisher Scientific (Shanghai).
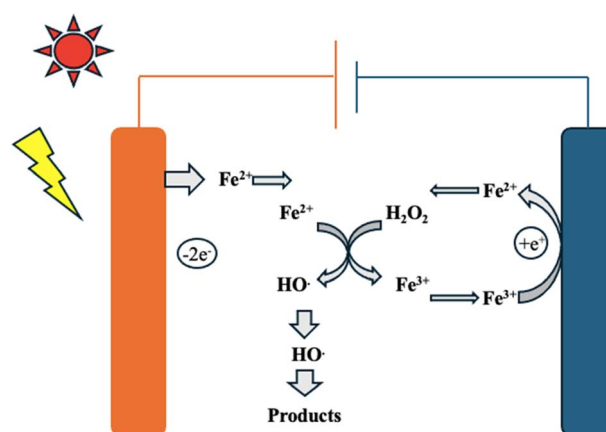

Fig. 1 Schematic diagram of photoelectric-Fenton reaction degradation mechanism.

2.2. Construction of the photoelectric-Fenton system

The photoelectric-Fenton system leverages the combined advantages of electrochemistry and photoreadiation to enhance its performance. Electrochemical methods are employed to generate Fe^{2+} and H_2O_2. During the electrolysis process, the iron anode undergoes an oxidation reaction, releasing Fe^{2+}, while the cathode produces H_2O_2 through a reduction reaction or bubble-mediated reduction of oxygen. These reactants rapidly combine to form highly reactive hydroxyl radicals ($^\cdot$OH). Additionally, a light source, typically with a wavelength range of 100–700 nanometers, is introduced. Photons interact with the components in the system, facilitating electron transitions. This interaction promotes the formation of radicals, effectively treating refractory compounds. The additions of Fe^{2+} and H_2O_2 affected the degradation efficiency in the photoelectric-Fenton system, so their addition amounts were optimized by comparing the molecular weights of the resulting products in this study.

2.3. Degradation of HA with the photoelectric-Fenton system

The photocatalytic reaction for HA degradation in a photoelectric-Fenton system was carried out by a CEL-HXF300-T3 system (Zhongjiao Jinyuan Science and Technology Co., Ltd, Beijing, China) equipped with a 500 W xenon lamp in the wavelength range of 300–2500 nm and no additional optical filters were used in this study (PerkinElmer, Waltham, MA, USA). HA (0.2 g) was dissolved in deionized water (100 mL) and magnetically stirred for 6 h at room temperature. A 0–0.5% H_2O_2 solution was added to the solution under stirring, and then 0–10 mmol of $FeSO_4$ and Fe $(CH_3COO)_3$ were added to the solution under stirring until uniformly distributed. The resulting solution was placed in an adapted reactor and a bias voltage of 0–2.5 V was applied. During the experiment, the solution was catalyzed for 20 min, and after determining the optimal conditions, the catalytic reaction was carried out in a photoelectric-Fenton system for 0–30 min, with samples taken at 5 min intervals. At the end of the reaction, the supernatants were lyophilized separately. The native, high-molecular-weight hyaluronic acid is referred to as 'HA', while the degradation products obtained from the photoelectric-Fenton system are termed 'DHA' (Degraded Hyaluronic Acid). The samples were named accordingly.

2.4. Removal and identification of iron ions

After the reaction of photoelectric-Fenton system, add ammonia to the solution and centrifuge it, take 5 mL of the solution after the reaction and put it in a test tube, add potassium thiocyanate (KSCN) and potassium ferrocyanide ($K_3Fe(CN)_6$) to the solution, and qualitatively identify the presence or absence of Fe^{2+} and Fe^{3+} in the solution according to the phenomenon change and color reaction.

2.5. Molecular weight determination

The molecular weights of the samples were analyzed by high-performance gel permeation chromatography (HPGPC) with a refractive index detector.[27] Separation occurred on TSK-gel G5000PW and G2500PWxl columns (7.8 mm × 30.0 cm each). Elution was conducted using 10 μL of ammonium acetate at 0.4 mL min^{-1}, calibrated with dextran standards of 5 kDa, 12 kDa, 25 kDa, 50 kDa, 150 kDa, 410 kDa, and 670 kDa.

2.6. Thin layer chromatography (TLC)

HA samples (2 mg mL^{-1}) and standards (glucose, lactose and β-cyclodextrin) were applied to 20 cm × 20 cm TLC plates from Macherey, Düren. The plates were developed with a solvent system of n-butanol, formic acid, and water (2 : 1 : 1 v/v/v) at 25 °C. After staining with digitonin, concentrated sulfuric acid, and methanol, the plates were heated to 105 °C to visualize bands.[28]

2.7. Measurement of HA content

The HA content in samples was quantified using the carbazole method.[29] Absorbance was measured at 530 nm using glucuronic acid as the standard. The HA content was calculated based on the standard curve.

2.8. Fourier-transform infrared (FTIR) spectroscopic analysis

The lyophilized samples were mixed with KBr powder. FTIR spectra were acquired at room temperature (21 ± 1 °C) using a Spectrum One-B FTIR spectrometer (PerkinElmer, Waltham, MA). The spectral range was 400 to 4000 cm^{-1}. To ensure accuracy, the background spectra were automatically subtracted using pure, dry potassium bromide (KBr), effectively eliminating any interference from atmospheric carbon dioxide and water vapor.[30]

2.9. Nuclear magnetic resonance (NMR) analysis

The HA sample (50 mg) was dissolved in 500 μL of D_2O (99.9%) and lyophilized twice. The ^1H NMR, of the HA sample was recorded on a Bruker Acsend 400 nuclear magnetic resonance instrument (Bruker, Rheinstetten, Germany).[31]

2.10. Analysis by high performance liquid chromatography-mass spectrometry

Oligosaccharide fragments were analyzed by HPLC-ESI-MSn.5 mg of DHA was mixed with 0.4 mL ammonia and 0.4 mL 0.3 mol L^{-1} PMP-methanol, vortexed, and nitrogen-blown in a light-proof bath at 70 °C for 30 min. Methanol was added, vortexed, and nitrogen-blown. This was repeated three times. The sample was washed three times with 1% acetic acid and trichloromethane, filtered through a 0.22 μm organic membrane, and analyzed by HPLC-MS/MS.[32]

The relative abundances of oligosaccharide fragments in the degradation products were determined based on the peak area percentages from HPLC-MS analysis, which provide a semi-quantitative comparison of the relative distribution of different oligosaccharide components rather than absolute concentrations.

For HPLC-PAD analysis, a TSKgel-Amide-80 column (20 mm × 150 mm, 3 μm) was used at 30 °C with a mobile phase of

20 mM ammonium acetate (pH 6) at 0.2 mL min^{-1}. Injection volume was 10 μL. For mass spectrometry, oligosaccharides were derivatized with PMP and analyzed on an LXQ mass spectrometer (Thermo Fisher, Pittsburgh, PA) with PDA and ESI. Separation was done on a TSKgel-Amide-80 column (4.6 mm × 150 mm, 3 μm) with a mobile phase of 20 mM ammonium acetate and acetonitrile (5 : 95 v/v) at 0.2 mL min^{-1}. ESI settings were 4.5 kV spray voltage, 37 V capillary voltage, and 275 °C capillary temperature. Data were processed using XCalibur software.

2.11. Investigation into the effects of HA and DHA on oxidative damage in Caco-2 cells

Caco-2 cells were cultured in DMEM medium supplemented with 100 U mL^{-1} penicillin, 1 μg mL^{-1} streptomycin, 10 μg mL^{-1} L-glutamine, and 20% fetal bovine serum (FBS) at 37 °C in a 5% CO$_2$ humidified incubator. Cell viability was assessed using the Tetrazolium Salt (MTT) assay. Briefly, cells were seeded in 96-well plates at a density of 2 × 10^4 cells per well and allowed to adhere for 24 hours. For the cytotoxicity assay, the culture medium (200 μL) was replaced with fresh medium containing various concentrations (0–800 μg mL^{-1}) of HA and DHA2 for another 24 hours.[33]

For the oxidative damage protection assay, after the initial 24 hour adhesion, cells were pretreated with 200 μL HA (200 μg mL^{-1}, 400 μg mL^{-1}, 600 μg mL^{-1}), DHA2 (200 μg mL^{-1}, 400 μg mL^{-1}, 600 μg mL^{-1}) for 24 hours. Subsequently, all groups except the blank control were exposed to 200 μL fresh DMEM containing 1.3 mM H$_2$O$_2$ for an additional 24 hours to induce oxidative damage.Then, 20 μL of MTT solution (5 mg mL^{-1}) was added to each well and incubated for 4 hours. The formazan crystals formed were then dissolved by adding 150 μL of dimethyl sulfoxide (DMSO) to each well after removing the supernatant. The absorbance of each well was measured at 570 nm using a microplate reader.

2.12. LC-MS metabolomics analysis

Caco-2 cells were plated at 2 × 10^5 cells well in a six-well plate and incubated for 24 hours. After supernatant removal, cells were treated with HA (200 μg mL^{-1}), DHA2-1 (400 μg mL^{-1}), or DHA2-2 (600 μg mL^{-1}) for 24 hours. Cells were then washed three times with PBS, exposed to 1.3 mM H$_2$O$_2$ for 24 hours and washed four more times. Intracellular metabolites were extracted using pre-cooled 80% methanol at low temperature, with undecanoic acid, nonadecanoic acid, and L-glutamic acid-d$_3$ (3.0 μg mL^{-1} each) as internal standards. The supernatant was collected by centrifuging at 12 000×g for 15 minutes at 4 °C and filtered through a 0.22 μm membrane for analysis.

The analytical platform comprised a Shimadzu high-performance liquid chromatography system and an AB 4000 QTRAP (AB Sciex, Massachusetts, USA). Chromatographic separation was performed on an XBridge BEH amide column (4.6 × 100 mm, 3.5 μm) with mobile phases A (20 mM ammonium acetate, pH 9) and B (acetonitrile). The column temperature was maintained at 40 °C. MRM settings for metabolites were based on Cao et al..[21]

2.13. Statistical analysis

All results were presented as mean ± SD. The data were analyzed utilizing SPSS 20.0 statistical software, and statistical significance between groups was considered at $p < 0.05$.

3. Results and discussion

3.1. Construction of the photoelectric-Fenton system for HA depolymerization

The photoelectric-Fenton system, as described in Section 2.2, was constructed and optimized for HA depolymerization. The additions of Fe^{2+} and H$_2$O$_2$ significantly affected the degradation efficiency, so their concentrations were optimized by comparing the molecular weights of the resulting products. Fig. 2A showed the effect of Fe^{2+} addition on the molecular weights of HA degradation products. The Fe^{2+} addition greatly enhanced the degradation efficiency, and the relative molecular weights of HA degradation product was as low as 3.5 kDa after 20 min when the Fe^{2+} additions were 8 mM. As exhibited by TLC in Fig. 2B, small molecules such as oligo and monosaccharides could be produced with Fe^{2+} concentrations ≥1 mM. Then, when the Fe^{2+} concentration was up to 8 mM, HA was almost catalyzed to small molecules as indicated by the faded original point. Of note, and the degradation efficiency of photoelectric-Fenton system with 10 mM Fe^{2+} was a little lower than that with 8 mM Fe^{2+}. So, 8 mM was considered as the optimal Fe^{2+} concentration for photoelectric-Fenton system to degrade HA (Table 1). Then the H$_2$O$_2$ addition amount was further optimized with 8 mM Fe^{2+}. As shown in Fig. 2C, the relative molecular mass of HA decreased, and the degradation rate heightened as the increase of H$_2$O$_2$ addition. Oligosaccharides could be observed when the H$_2$O$_2$ addition was ≥0.1% and HA were catalyzed thoroughly with the H$_2$O$_2$ addition of 0.5% (Fig. 2D). Moreover, Table 1 reflects that the uronic acid content, which reflected the total content of HA and its degradation products containing uronic acid, decreased alone with degradation proceeding. Thus, with the optimal conditions (8 mM of Fe^{2+} and 0.5% of H$_2$O$_2$ addition), the photoelectric-Fenton system could obtain a yield of 47.29% for HA degradation.

With the optimal conditions, the changes of HA within 30 min degradation were monitored. The relative molecular weight of HA decreased significantly after 5 min degradation while the molecular weight was below the limit of HPGPC after 20 min (Fig. 3A). Then the TLC analysis (Fig. 3B) showed that oligosaccharide products was obviously enriched after 10 min degradation, and more and more HA was catalyzed gradually. However, it is worth noting that the uronic acid content decreased in conjunction with the degradation process. The above experimental results further showed that the addition of Fe^{2+} and photo electrocatalysis constituting the photoelectric-Fenton system could effectively reduce the relative molecular mass of HA. The introduction of the Fenton system largely improved the degradation efficiency of HA.

Fenton oxidative degradation is one of the most commonly applied oxidative degradation methods.[25,26] Li et al.[32] applied a Cu^{2+} induced Fenton like system to degrade chondroitin sulfate. Renato M et al.[15] used the Fenton reaction to prepare
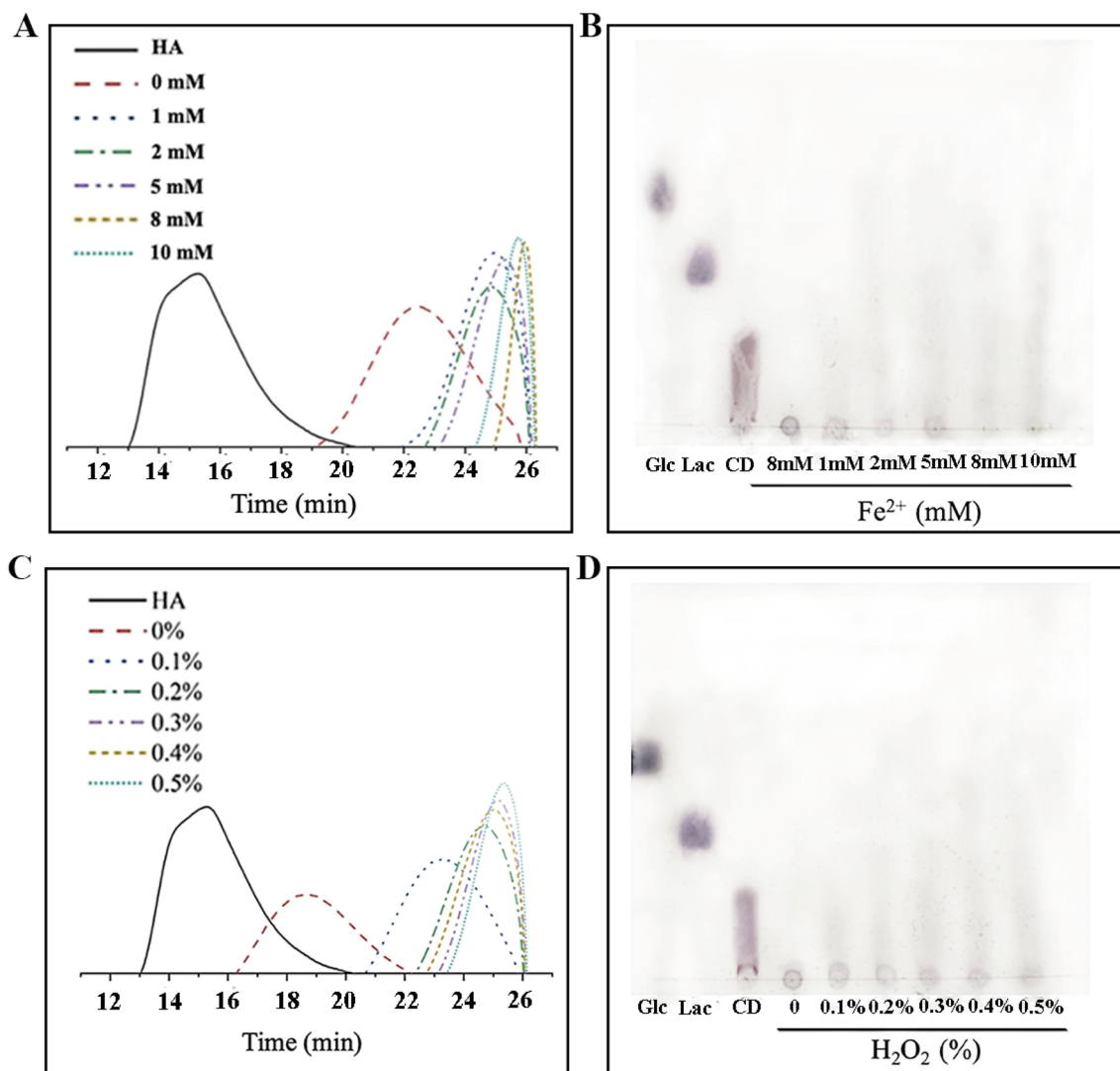
Fig. 2 Degraded HA molecular weight (Mw) in response to Fe^{2+} (A and B) and H_2O_2 (C and D) addition. TLC analysis at varying concentrations is shown in (B) and (D).

low-molecular-weight heparin and found that the pentose sequence in heparin was not destroyed during degradation. A comparative experiment under identical conditions (8 mM Fe^{2+}, 0.5% H_2O_2) revealed that the photoelectric-Fenton system achieved a much higher degradation rate (reaching 1.6 kDa in 25 min) than the conventional Fenton process, highlighting the critical role of photoelectric assistance in enhancing $\cdot OH$ yield and Fe^{2+}/Fe^{3+} cycling efficiency.[33,34] Then the present study demonstrated that the introduction of a Fenton system on the basis of photo electrocatalysis can significantly increase the degradation efficiency.

3.2. Characterization of degradation products by FTIR and NMR spectroscopy

In order to determine the structural changes of HA after degradation by the photoelectric-Fenton system FTIR and ^1H NMR spectra of HA and its degradation products, DHA1 and DHA2, were analyzed and compared. The FTIR spectra of DHA1

and DHA2 showed great similarities as that of HA (Fig. 4A), and they both demonstrated characteristic peaks at around 3304 cm^{-1} (O–H stretching).[35] Additionally, the carboxylate anion of glucuronic acid undergoes stretching vibration, resulting in the production of an absorption band in the vicinity of 1615 cm^{-1}.[36] The photoelectric-Fenton degradation did not change the structural units of HA. As shown in Fig. 4B, the signal at 1.97 ppm could be assigned to the methyl proton of GlcNAc, and the signals between 3.9 ppm and 3.0 ppm were due to the protons of sugar rings. Moreover, the signals at 4.35 ppm and 4.45 ppm were in general agreement with those reported for the isomeric protons of GlcA and GlcNAc, respectively.[37] DHA1 and DHA2 both showed the signals of HA, but there were additional signals at around 1.80 ppm and 1.15 indicating the presence of short chain fatty acids, such as acetic acid and propionic acid. Notably, acetic acid and propionic acid are common products of uronic acid oxidation. Notably, the ^1H NMR spectrum of DHA2 showed high resolution due to its lower molecular weight and viscosity.[38] Thus, the FTIR and ^1H NMR

Table 1 Molecular weight and uronic acid contents of HA degradation products with different conditions[a]

Reaction condition			Mw (kDa)	Uronic acid (%)
Fe^{2+} (mM)	0	0.5% H_2O_2 20 min	37.1	50.89 ± 0.92^a
	1		8.4	48.62 ± 0.80^a
	2		7.2	48.99 ± 0.92^a
	5		5.8	49.90 ± 0.80^a
	8		3.5	37.43 ± 0.78^b
	10		4.1	38.42 ± 1.87^b
H_2O_2 (%)	0	8 mM Fe^{2+} 20 min	46.1	51.80 ± 2.01^a
	0.1		22.6	51.97 ± 0.72^a
	0.2		7.8	50.92 ± 0.91^{ab}
	0.3		6.6	49.13 ± 1.31^{ab}
	0.4		5.9	48.10 ± 0.58^{ab}
	0.5		5.2	47.29 ± 2.59^b
Time (min)	0	0.5% H_2O_2 8 mM Fe^{2+}	> 800	55.41 ± 0.99^a
	5		18.5	47.15 ± 0.53^b
	10		6.7	41.64 ± 0.24^b
	15		3.9	34.49 ± 1.93^c
	20		1.7	33.02 ± 0.62^c
	25		1.6	24.77 ± 0.61^d
	30		1.5	21.91 ± 0.43^d

[a] Note. different letters in the same column indicate significant differences ($p < 0.05$).

analysis results indicated the photoelectric-Fenton system could depolymerize HA without significantly alerting its structural block but still yield some byproducts.[39]

3.3. Identification of oligosaccharide fragments in degradation products

To investigate the oligosaccharide fragment structure of DHA2 after degradation by the photoelectric-Fenton system, the HPLC-ESI-MSn method was utilized. In MS^2 (Fig. 5A), pseudo-molecular ions were detected at m/z 1283 $[M + H]^+$, m/z 1107 $[M\text{-}GlcA + H]^+$, m/z 904 $[M\text{-}GlcA\text{-}GlcNAc + H]^+$, and m/z 728 $[M\text{-}GlcA\text{-}GlcNAc\text{-}GlcA + H]^+$, leading to the identification of the peak as the PMP derivative of GlcA → GlcNAc → GlcA → GlcNAc → GlcA. Moreover, in MS_2 (Fig. 5B), the pseudo-

molecular ion peak at m/z 1107 $[M + H]^+$ generated fragment ions at m/z 904 $[M\text{-}GlcNAc + H]^+$ and m/z 728 $[M\text{-}GlcNAc\text{-}GlcA + H]^+$ confirming the structure as the PMP derivative of GlcA → GlcNAc → GlcA → GlcNAc. Additional analysis revealed pseudo-molecular ions at m/z 1077 $[M + H]^+$, m/z 874 $[M\text{-}GlcNAc + H]^+$, and m/z 698 $[M\text{-}GlcNAc\text{-}GlcA + H]^+$ in MS^2 (Fig. 5C). The pseudo-molecular ion at m/z 904 $[M + H]^+$ generated a fragment ion at m/z 728 $[M\text{-}GlcA + H]^+$, identifying this peak as the PMP-labeled GlcA → GlcNAc → GlcA (Fig. 5D). Similarly, m/z 874 $[M + H]^+$ produced a fragment ion at m/z 698 $[M\text{-}GlcA + H]^+$ in MS^2, corresponding to the PMP-labeled GlcA → GlcNAc → GlcA (Fig. 5E). Moreover, m/z 728 $[M + H]^+$ at the pseudo-molecular ion peak in MS^2 generated a fragment ion at m/z 525 $[M\text{-}GlcNAc + H]^+$ (Fig. 5F), while m/z 698 $[M + H]^+$ produced a fragment ion at m/z 495 $[M\text{-}GlcA + H]^+$ (Fig. 5G).

The photoelectric-Fenton system facilitated the oxidative reaction of the reducing end of GlcA, resulting in the shedding of CH_2O during the degradation of HA and the formation of AraA (Adenine arabinoside) as the reducing end. Table 2 presents the peak area ratios of different oligosaccharide fragments in the DHA2 ion chromatograms of the degradation products, with reducing ends of GlcA (Glucuronic acid) and AraA. Almost no deacetylated products were detected, indicating minimal deacetylation during the process. The highest amount of oligosaccharide fragments was observed at m/z 728 (64.33%), while the lowest amount was detected at m/z 874 (4.23%).

3.4. Protective effects of HA and DHA2 against cellular oxidative damage

To investigate the protective effects of hyaluronic acid (HA) of two molecular weights against oxidative damage in intestinal epithelial cells, an in vitro study was conducted using a Caco-2 cell model induced by H_2O_2. The native, high-molecular-weight HA (>800 kDa) was compared with its low-molecular-weight degradation product, DHA2 (1.6 kDa), obtained after 25 min of treatment under optimal conditions (8 mM Fe^{2+}, 0.5% H_2O_2). Initially, the MTT assay was employed to assess the cytotoxicity of both HA and DHA2 on the cells. The results
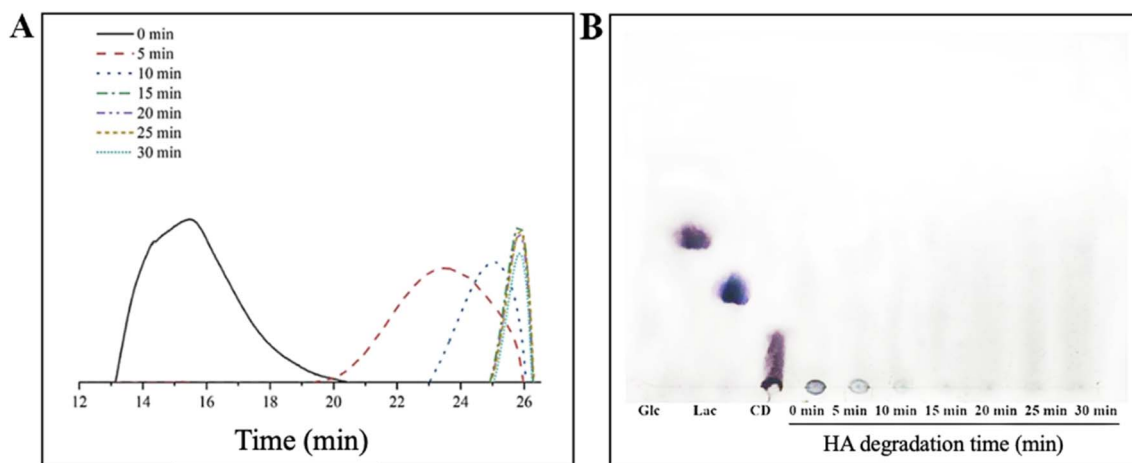

Fig. 3 Molecular weight distribution (A) and TLC analysis (B) of hyaluronic acid at different degradation times following the addition of 8 mM Fe^{2+} and 0.5% H_2O_2.
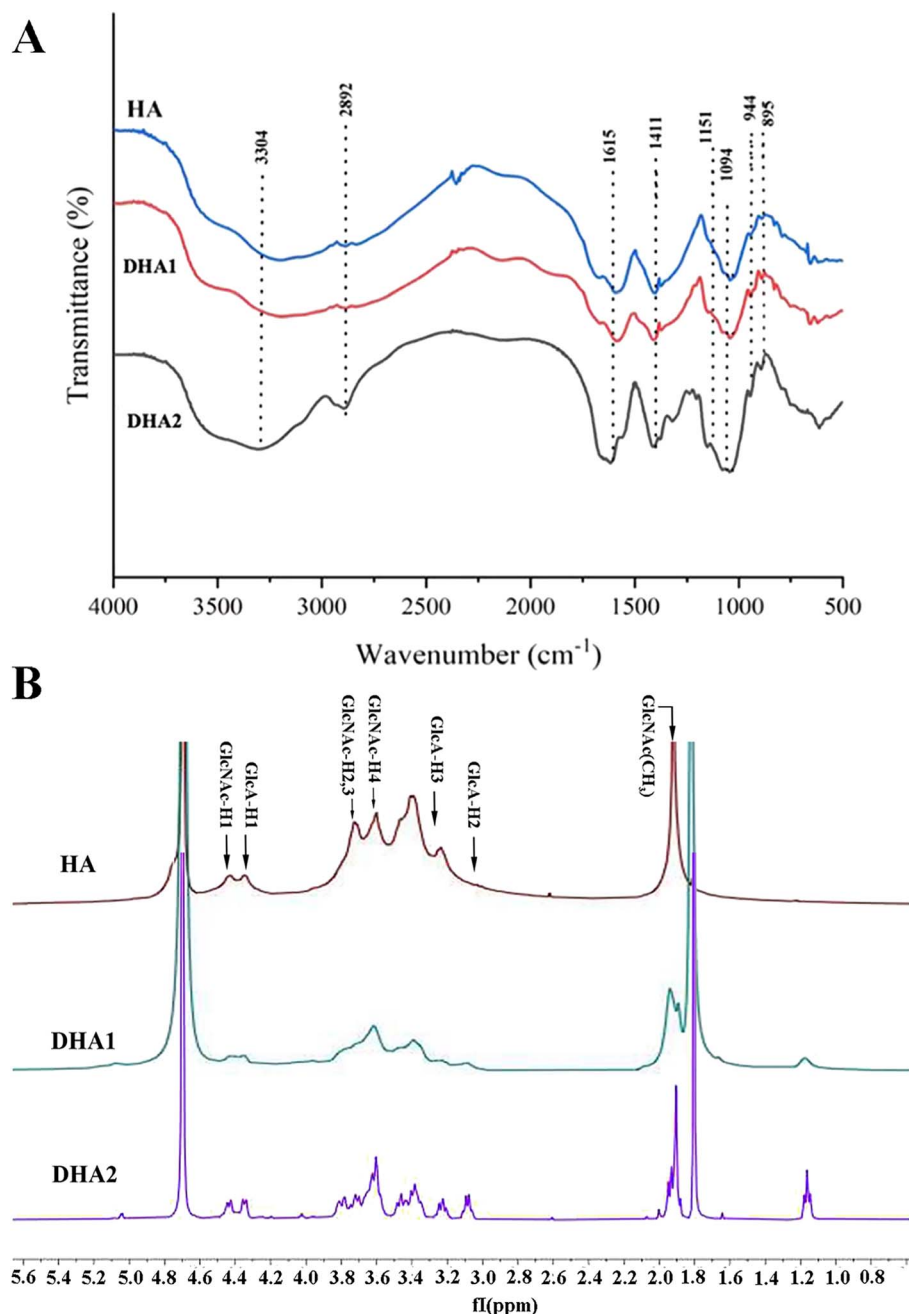
Fig. 4 FT-IR spectra (A) and ^1H NMR spectra (B) of hyaluronic acid and its degradation products.

indicated that neither HA nor DHA2 exhibited significant toxicity at various concentrations tested (Fig. 6A and B). Furthermore, these findings also suggested that the improvement observed in cellular oxidative damage by HA and DHA2 was not mediated through the promotion of cell proliferation, thereby enhancing cell survival rates.

Excessive H_2O_2 could entry into cells induces oxidative stress, causing cellular oxidative damage,[40,41] so it was selected as the inducer to create a Caco-2 cell model of oxidative damage.[42] The MTT method was then used to examine the protective effects of HA and DHA2 against H_2O_2 induced

oxidative damage in Caco-2 cells, and the results, illustrated in Fig. 6C and D. The results revealed that both HA and DHA2 treatments significantly enhanced the survival rate of intestinal epithelial cells exposed to H_2O_2, indicating their protective effects against oxidative damage. Currently, extensive research has demonstrated that various functional polysaccharides possess antioxidant properties. Chaiklahan R et al.[8] experimentally verified that polysaccharide extracts from Spirulina at 90 °C contained high phenolic content and exhibited good antioxidant capacity. Kan Y et al.[13] extracted polysaccharides from the fruiting bodies of Ganoderma lucidum using ultrafine
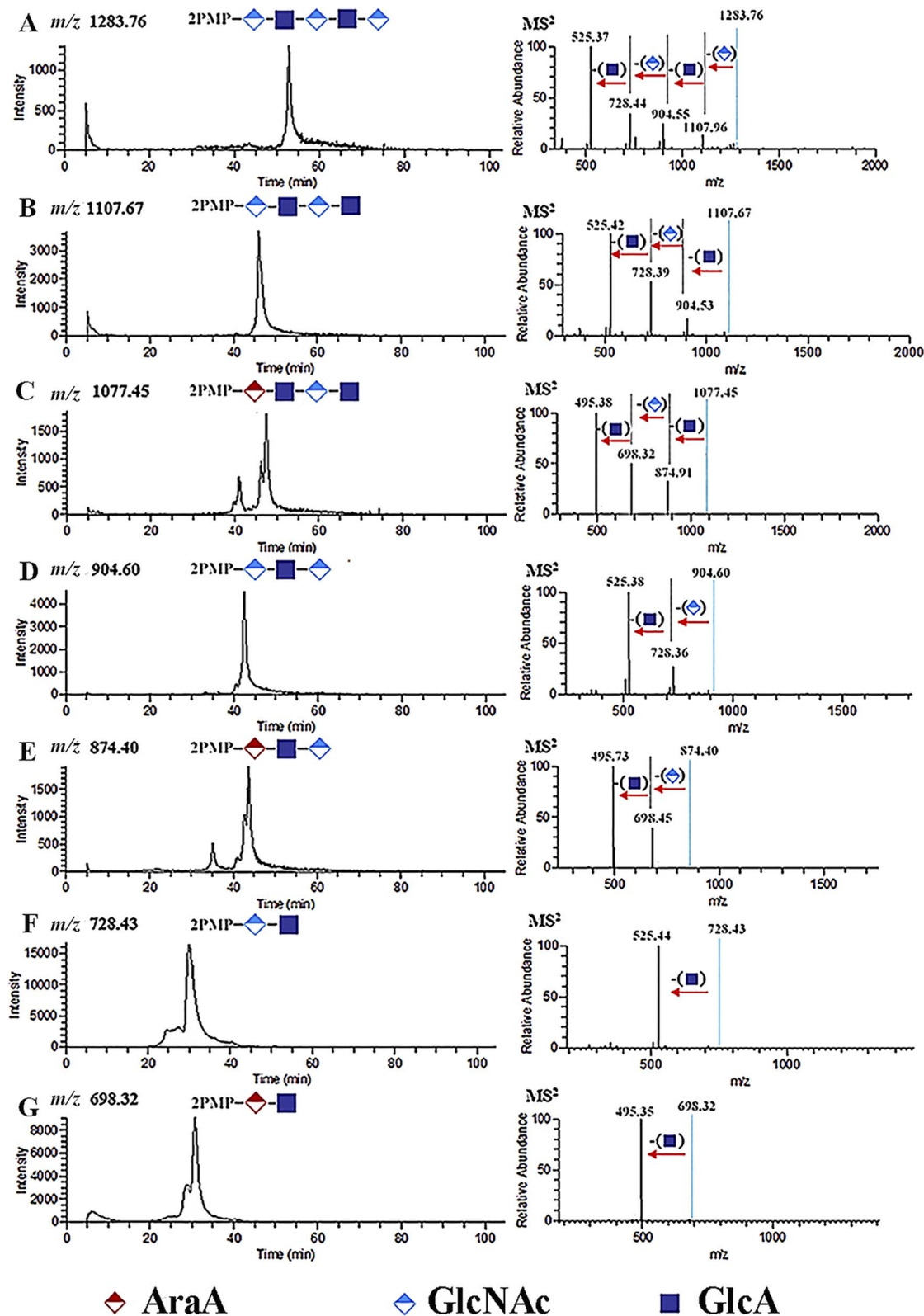
Fig. 5 Extracted-ion chromatograms and MS^2 of PMP-labeled oligosaccharides in DHA2.

pulverization technology and conducted antioxidant validation, showing that polysaccharides derived from Ganoderma lucidum exhibit potent reducing power, DPPH radical scavenging ability, and oxygen radical scavenging capacity. In recent years, as marine resources have been increasingly explored and utilized, a multitude of polysaccharides possessing antioxidant

Table 2 Oligosaccharides of hyaluronic acid and its degradation products[a]

No.	Retention time (min)	m/z	Oligosaccharide	Area preparation (%)
1	52.9	1283	GlcA → GlcNAc → GlcA → GlcNAc → GlcA	5.1
2	45.9	1107	GlcA → GlcNAc → GlcA → GlcNAc	4.6
3	40.9/47.4/46.2	1077	AraA → GlcNAc → GlcA → GlcNAc	4.8
4	40.7/42.4	904	AraA → GlcNAc → GlcA	8.6
5	35.2/43.6	874	GlcA → GlcNAc → GlcA	4.2
6	29.9	728	GlcA → GlcNAc	64.3
7	28.7/30.7	698	AraA → GlcNAc	8.3

[a] Note. values represent mean ± SD ($n = 3$) of peak area percentages (%), which indicate the relative distribution of each oligosaccharide component in the degradation products rather than absolute concentrations.
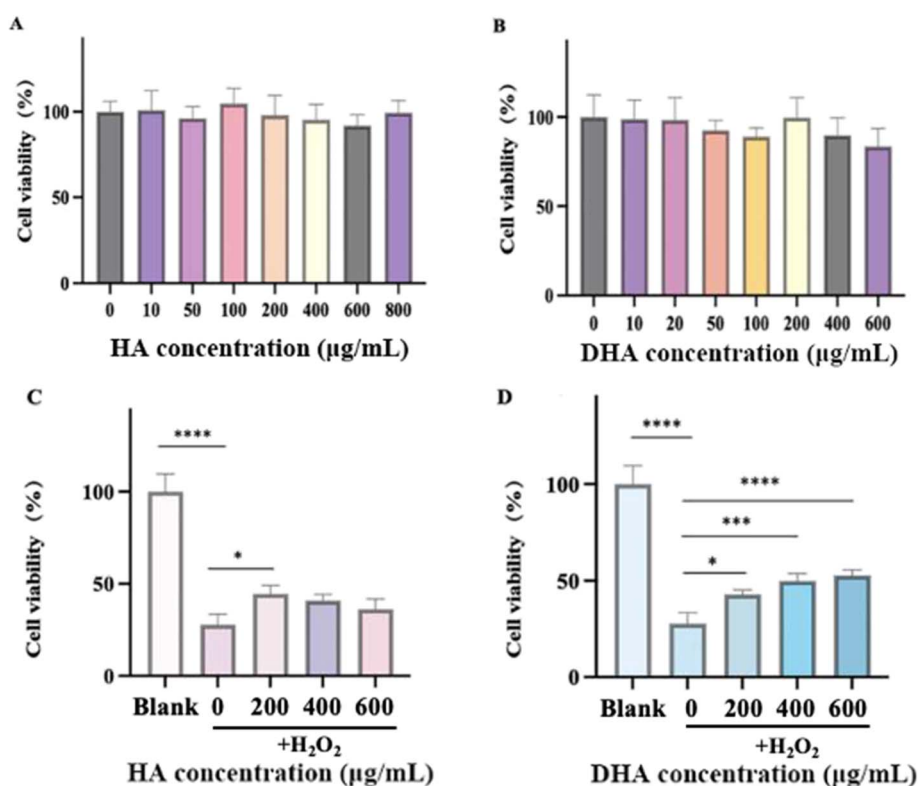

Fig. 6 Effect of HA (A) and DHA2 (B) on cell viability and protective effect of HA (C) and DHA2 (D) against cellular oxidative damage. Values are expressed as mean ± standard deviation ($n = 6$), *$p < 0.05$, ***$p < 0.001$ and ****$p < 0.0001$.

activity have been identified in brown algae, green algae, and red algae.[42–44] Functional polysaccharides hold promising prospects in the field of antioxidant damage protection.

3.5. Regulation of metabolism in Caco-2 cells by HA and DHA

PLS-DA analysis showed clear separation between the control and H_2O_2 groups (Fig. 7A). The HA + H_2O_2, DHA2-1 + H_2O_2, and DHA2-2 + H_2O_2 groups were distant from the H_2O_2 group and, compared to the H_2O_2 group, were closer to the blank control group. This suggests that both HA and DHA2 can improve H_2O_2-induced cellular oxidative damage by regulating intracellular metabolite levels. Notably, DHA2 exhibited a better

improvement effect than HA. To gain a more profound understanding of the protective effects of HA and DHA2 against oxidative damage in intestinal epithelial cells, a method based on LC-MS/MS was utilized for the analysis of metabolites in Caco-2 cells. Two concentrations of DHA2, termed DHA2-1 (400 μg mL^{-1}) and DHA2-2 (600 μg mL^{-1}), were chosen for the study. By applying a statistical analysis with a significance level set at $p < 0.05$, the metabolites between the control group and the H_2O_2-treated group were compared, and totally 36 differential compounds were identified. Compared to the H_2O_2 group, the levels of 23, 18, and 22 metabolites in the HA, DHA2-1, and DHA2-2 groups, respectively, returned to those of the normal group (Fig. 7B).
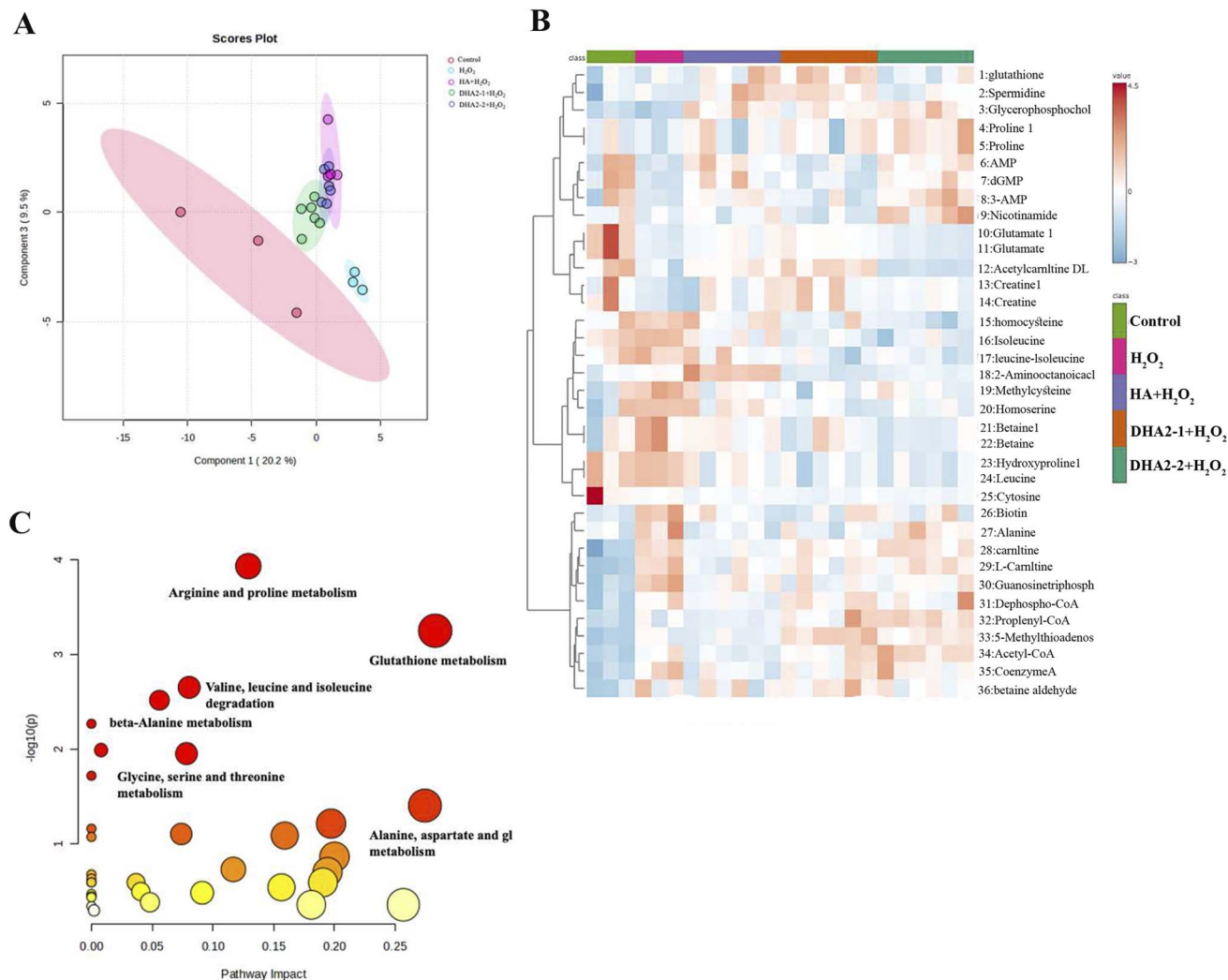
Fig. 7 PLS-DA analysis of metabolite profiles groups (A) and heatmap of the differential metabolites among different groups (B). These metabolites related metabolic pathways (C).

By utilizing the KEGG database to analyze the relevant metabolic pathways, it was found that H_2O_2 treatment significantly affected arginine and proline metabolism, and glutathione metabolism (Fig. 7C). Furthermore, it influenced the degradation of valine, leucine, and isoleucine, along with the metabolism of glyoxylate and dicarboxylic acids, nitrogen metabolism, β-alanine metabolism, glycine, aspartate, and glutamate metabolism, alanine, aspartate, and glutamate metabolism, biosynthesis of leucine and isoleucine, and biosynthesis of arginine. These findings indicate that H_2O_2 stimulation can notably influence specific amino acid metabolic pathways within the cells. Analyzing the two primary metabolic pathways, compared to the blank control group, there were significant differences in the levels of six metabolites in the H_2O_2 group (Fig. 8A and B). H_2O_2 treatment significantly increased the content of spermidine, acetyl-CoA and significantly decreased the levels of L-proline, hydroxyproline, creatine and L-glutamic acid.

Current research indicates that significant alterations occur in intracellular amino acid metabolism following H_2O_2

stimulation, leading to oxidative damage.[44] Consequently, changes in metabolite levels were analyzed to elucidate the mechanisms by which HA and DHA ameliorated oxidative damage.[45] Glutamic acid is crucial for amino acid, protein, and nucleotide synthesis. Arginine and proline metabolism may be related to mitochondrial dysfunction and ROS scavenging. The H_2O_2 group showed decreased glutamic acid, suggesting inhibition of signal transduction and proliferation in Caco-2 cells. Glutamic acid reacts with ammonia to produce glutamine and can release ammonia to form α-ketoglutarate. Ammonia is used in the urea cycle, while α-ketoglutarate enters the TCA cycle. Glutamic acid metabolism is linked to the TCA cycle and nitrogen balance.[46] Glutamine stimulates cell division, serves as a carbon source for energy production, and is a precursor for metabolite synthesis. The research indicates that H_2O_2-induced cell injury leads to reduced cell proliferation and viability, accompanied by downregulation of glutamic acid metabolism, suggesting impaired cell energy metabolism. Valine and leucine, as branched-chain amino acids, play a key role in energy metabolism and ensure long-term energy supply.[47]
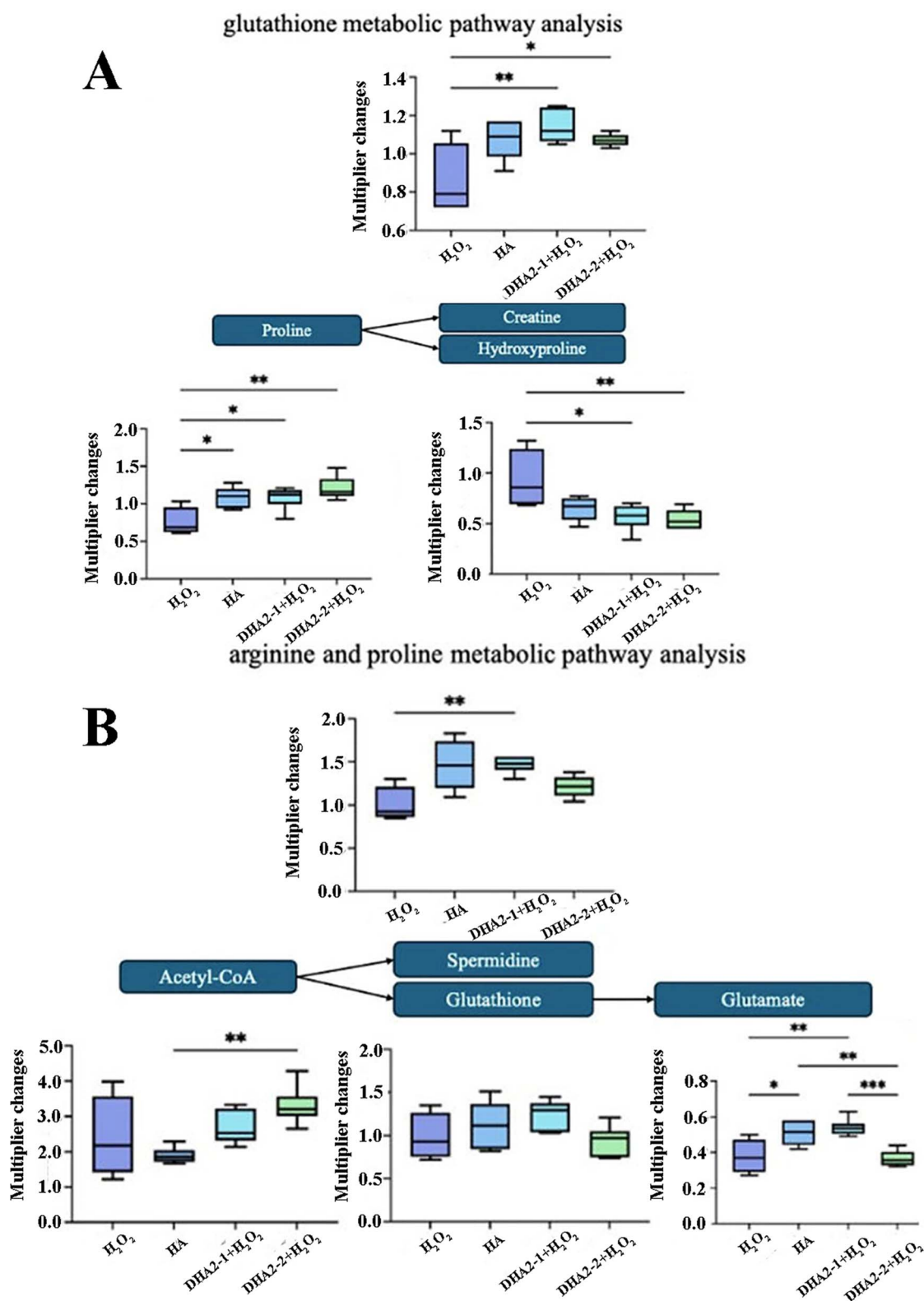
Fig. 8   Glutathione metabolic pathway analysis(A) and arginine and proline metabolic pathway analysis (B). These results were represented as mean ± SD ($n = 6$). *$p < 0.05$, **$p < 0.01$, and ***$p < 0.001$ by the Tukey HSD test.

Altered biosynthesis of valine, leucine, and isoleucine indicates disruption in energy metabolism. In mitochondria, pyruvate oxidation to acetyl-CoA is crucial for entering the TCA cycle, highlighting acetyl-CoA's pivotal role in transforming sugars, fats, and amino acids in the body. The presence of accumulated acetyl-CoA suggests disruptions in the TCA cycle and the

synthesis of sugars and lipids. In the HA or DHA2 groups, the levels of these metabolites were partially reversed, suggesting that treatment with hyaluronic acid of different molecular weights can alleviate cellular oxidative damage by improving arginine and proline metabolism as well as glutathione metabolism pathways.

The modulation of arginine and proline metabolism pathways by HA and DHA2 may involve receptor-mediated signaling, as low-molecular-weight hyaluronic acid is a known ligand for receptors including TLR4 and CD44.[48] Activation of these receptors can initiate downstream signaling cascades, such as those involving Nrf2 and NF-κB, potentially leading to the upregulation of antioxidant enzymes and stabilization of metabolic networks.[49,50] In addition, DHA2 may exert direct antioxidant effects by scavenging reactive oxygen species, thereby reducing oxidative stress and mitigating H_2O_2-induced disruption of mitochondrial function and the TCA cycle—processes integral to amino acid metabolism. It is also plausible that HA and DHA2 influence the expression or activity of key metabolic enzymes within these pathways. Further studies are needed to clarify the specific mechanisms of modulation, particularly through detailed investigations of protein expression and molecular interactions.

The protective effect of DHA2 on intestinal epithelial cells supports its potential biomedical relevance, particularly in conditions linked to oxidative damage such as inflammatory bowel disease.[51] By alleviating oxidative stress and helping restore metabolic balance, DHA2 could be suited for development as a nutraceutical or therapeutic agent aimed at supporting mucosal healing and managing IBD symptoms. Moreover, the low molecular weight of DHA2 suggests favorable oral bioavailability, making it a promising candidate for oral formulations targeting gut health and inflammatory regulation.

4. Conclusions

The present study developed a photoelectric-Fenton catalytic degradation method for HA depolymerization and investigated the effects of Fe^{2+} and H_2O_2 addition amounts on degradation efficiency. The results indicated that the optimal conditions for photo electrocatalytic degradation were 8 mM Fe^{2+} addition and 0.5% H_2O_2 addition. A comparison of the chemical compositions of the degradation products DHA1 and DHA2 with that of HA revealed the degradation did not change their structural blocks significantly, and pentasaccharide, tetrasaccharide, trisaccharide, and disaccharide fragments were identified in the degradation product DHA2. Moreover, *in vitro* experiments using Caco-2 cells showed that both HA and DHA2 had protective effects against oxidative damage, with DHA2 exhibiting superior efficacy to HA.

The enhanced antioxidant activity of DHA2 observed in this study aligns with the general structure–activity relationships reported for bioactive polysaccharides. Similar to our findings on HA, studies on sulfated polysaccharides like fucoidan have demonstrated that controlled depolymerization to low molecular weight fragments can significantly enhance specific bioactivities, particularly antioxidant capacity.[52] For instance, enzymatic or radical depolymerization of fucoidan from brown seaweeds yields low molecular weight fucans (LMWFs) with improved antioxidant properties compared to their native polymers.[53] However, a notable difference lies in the primary mechanism of action. While the antioxidant activity of sulfated polysaccharides like fucoidan is often strongly correlated with their sulfate content and position, the activity of LMW-HA derivatives such as DHA2 is primarily attributed to factors like increased number of reducing ends, enhanced bioavailability due to lower viscosity, and improved cellular uptake.[54] Furthermore, similar to reports on LMW fucoidan[55] and other degraded polysaccharides, our metabolite analysis suggests that the protective effects of DHA2 extend beyond direct radical scavenging to include the modulation of critical cellular metabolic pathways (*e.g.*, arginine and proline metabolism) under oxidative stress. This underscores a convergent biological strategy where low molecular weight polysaccharides, regardless of specific type, can effectively regulate intracellular antioxidant defense systems.

In addition, HA and DHA2 modulated the arginine and proline metabolic pathways by upregulating the content of hydroxyproline and downregulating the levels of L-proline, creatinine, spermidine, L-glutamic acid, and acetyl-CoA, thereby mitigating oxidative damage. These findings, combined with insights from studies on other functional polysaccharides,[56] suggest that photoelectric-Fenton-derived LMW-HA holds great potential as an effective antioxidant agent for applications in functional foods, nutraceuticals, and biomedical formulations aimed at mitigating oxidative stress related damage.

Author contributions

Jiayi Yan: conceptualization, investigation, data curation, writing – original draft. Youxian Zhou: investigation, supervision. Chen Song: investigation, methodology. Yunning Yang: investigation, visualization. Fanhua Kong: methodology, formal analysis, validation. JingfengYang: resources, investigation. Shuang Song: conceptualization, supervision, writing – review & editing, project administration, funding acquisition.

Conflicts of interest

Authors have no conflicts of interest.

Data Availability

All data supporting this study are included in the article and its SI.

Acknowledgements

References

1 J. Fang, D. Wang, H. Xu, *et al.*, Unleashing solar energy's full potential: Synergetic thermo-photo catalysis for enhanced

hydrogen production with metal-free carbon nitrides, *Energy Convers. Manage.*, 2024, **300**, 117995.

2 A. Mahdi, M. Arshadi and M. Baghdadi, Treatment of molasses-based alcohol distillery wastewater using Electro-Fenton oxidation: Optimization and model prediction by response surface methodology, *J. Environ. Manage.*, 2024, **372**, 123221.

3 K. Hasani, A. Peyghami, A. Moharrami, *et al.*, The efficacy of sono-electro-Fenton process for removal of Cefixime antibiotic from aqueous solutions by response surface methodology (RSM) and evaluation of toxicity of effluent by microorganisms, *Arab. J. Chem.*, 2020, **13**(7), 6122–6139.

4 J. M. Cyphert, C. S. Trempus and S. Garantziotis, Size matters: molecular weight specificity of hyaluronan effects in cell biology, *Int. J. Cell Mol. Biol.*, 2015, **2015**(1), 563818.

5 J. Lv, Q. Zhao, J. Jiang, *et al.*, Sludge dewaterability improvement with microbial fuel cell powered electro-Fenton system (MFC EFs): Performance and mechanisms, *Sci. Total Environ.*, 2024, **923**, 171422.

6 Q. Wen, F. Kong, H. Zheng, *et al.*, Simultaneous processes of electricity generation and ceftriaxone sodium degradation in an air-cathode single chamber microbial fuel cell, *J. Power Sources*, 2011, **196**(5), 2567–2572.

7 E. Fischer, T. P. Callaghan, F. Heatley, *et al.*, Shear flow affects secondary and tertiary structures in hyaluronan solution as shown by rheo -NMR, *J. Mol. Struct.*, 2002, 602303.

8 R. Chaiklahan, N. Chirasuwan, P. Triratana, *et al.*, Polysaccharide extraction from *Spirulina* sp. and its antioxidant capacity, *Int. J. Biol. Macromol.*, 2013, **58**, 73–78.

9 Y. Chen, S. Fei, X. Yu, *et al.*, Dandelion (*Taraxacum mongolicum*) Extract Alleviated H_2O_2-Induced Oxidative Damage: The Underlying Mechanism Revealed by Metabolomics and Lipidomics, *Foods*, 2023, **12**(17), 3314.

10 A. Mahdi, M. Arshadi and M. Baghdadi, Treatment of molasses-based alcohol distillery wastewater using Electro-Fenton oxidation: Optimization and model prediction by response surface methodology, *J. Environ. Manage.*, 2024, **372**, 123221.

11 M. Renato, J. M. Carlos, A. Hugo, *et al.*, Photoelectrocatalytic degradation of 2,4-dichlorophenol in a TiO_2 nanotube-coated disc flow reactor, *Chemosphere*, 2021, 268.

12 V. Ruiz, Z. E. Ilhan, D. W. Kang, *et al.*, The source of inoculum plays a defining role in the development of MEC microbial consortia fed with acetic and propionic acid mixtures, *J. Biotechnol.*, 2014, **182**, 11–18.

13 Y. Kan, T. Chen, Y. Wu, *et al.*, Antioxidant activity of polysaccharide extracted from *Ganoderma lucidum* using response surface methodology, *Int. J. Biol. Macromol.*, 2015, **72**, 151–157.

14 A. Asari, T. Kanemitsu and H. Kurihara, Oral administration of high molecular weight hyaluronan (900 kDa) controls immune system *via* Toll-like receptor 4 in the intestinal epithelium, *J. Biol. Chem.*, 2010, **285**(32), 24751–24758.

15 M. Renato, J. M. Carlos, A. Hugo, *et al.*, Photoelectrocatalytic degradation of 2,4-dichlorophenol in a TiO_2 nanotube-coated disc flow reactor, *Chemosphere*, 2021, 268.

16 A. N. Seresht, M. Moradkhan, T. A. Sareshkeh, *et al.*, Hybrid of photoelectrocatalysis and membrane processes as an efficient combination in pollutant removal from wastewaters: A review, *Sep. Purif. Technol.*, 2025, **377**(P2), 134286–134286.

17 A. M. B. Hasan, N. T. Tuan, Z. Ming, *et al.*, In vitro fermentation of *Gracilaria lemaneiformis* and its sulfated polysaccharides by rabbitfish gut microbes, *Int. J. Biol. Macromol.*, 2023, **246**, 125561.

18 J. R. Dodd, D. C. Blundell, M. B. Sattelle, *et al.*, Chemical modification of hyaluronan oligosaccharides differentially modulates hyaluronan-hyaladherin interactions, *J. Biol. Chem.*, 2024, **300**(9), 107668.

19 P. Bautista, F. A. Mohedano, A. J. Casas, *et al.*, An overview of the application of Fenton oxidation to industrial wastewaters treatment, *J. Chem. Technol. Biotechnol.*, 2008, **83**(10), 1323–1338.

20 J. R. E. Fraser, T. C. Laurent and U. B. G. Laurent, Hyaluronan: its nature, distribution, functions and turnover, *J. Intern. Med.*, 1997, **242**(1), 27–33.

21 C. Cao, L. L. Wang, C. Q. Ai, *et al.*, Impact of *Lycium barbarum* arabinogalactan on the fecal metabolome in a DSS-induced chronic colitis mouse model, *Food Funct.*, 2022, **13**, 8703–8716.

22 J. Liu, R. Liang, Z. Hu, *et al.*, Photoelectrocatalysis/photoelectro-Fenton system based on cone-like TiO_2/nickel foam photoanode for efficient degradation of carbamazepine: Comparison with DSA, *Chem. Eng. J.*, 2024, **491**, 152088.

23 N. Hisada, H. Satsu, A. Mori, *et al.*, Low-molecular-weight hyaluronan permeates through human intestinal Caco-2 cell monolayers *via* the paracellular pathway, *Biosc. Biotech. Biochem.*, 2008, **72**(4), 1111–1114.

24 Y. Sambuy, I. De Angelis, G. Ranaldi, *et al.*, The Caco-2 cell line as a model of the intestinal barrier: influence of cell and culture-related factors on Caco-2 cell functional characteristics, *Cell Biol. Toxicol.*, 2005, **21**(1), 1–26.

25 K. Qin, F. Wang, R. M. L. Simpson, *et al.*, Hyaluronan promotes the regeneration of vascular smooth muscle with potent contractile function in rapidly biodegradable vascular grafts, *Biomaterials*, 2020, **257**, 120226.

26 F. Alanah and B. G. J. I. Patricia, Electrochemical technologies combined with physical, biological, and chemical processes for the treatment of pollutants and wastes: A review, *J. Environ. Chem. Eng.*, 2022, **10**, 107810.

27 Y. Wang, F. Wang and X. Guo, Comparison of three methods for determining the relative molecular weight of low molecular weight hyaluronic acid, *Chin. J. Biochem. Pharm.*, 2007, (3), 182–184.

28 C. Ke, D. Qiao and X. Zeng, Study on preparation and antioxidant activity of low molecular weight hyaluronic acid, *Sci. Technol. Food Ind.*, 2010, (01), 107–111.

29 T. Bitter and H. M. Muir, A modified uronic acid carbazole reaction, *Anal. Biochem.*, 1962, **4**(4), 330–334.

30 K. Y. Choi, S. Lee, K. Park, *et al.*, Preparation and characterization of hyaluronic acid-based hydrogel

nanoparticles, *J. Phys. Chem. Solids*, 2008, **69**(5–6), 1591–1595.

31 E. Fischer, P. T. Callaghan, F. Heatley, *et al.*, Shear flow affects secondary and tertiary structures in hyaluronan solution as shown by rheo-NMR, *J. Mol. Struct.*, 2002, **602**, 303–311.

32 J. Li, S. Li, Z. Zhi, *et al.*, Depolymerization of fucosylated chondroitin sulfate with a modified fenton-system and anticoagulant activity of the resulting fragments, *Mar. Drugs*, 2016, **14**(9), 170.

33 Y. Chen, S. Fei, X. Yu, *et al.*, Dandelion (Taraxacum mongolicum) Extract Alleviated H2O2-Induced Oxidative Damage: The Underlying Mechanism Revealed by Metabolomics and Lipidomics, *Foods*, 2023, **12**(17), 3314.

34 R. Weronika, M. Arnold, R. Aleksandra, *et al.*, Alterations in fecal short chain fatty acids (SCFAs) and branched short-chain fatty acids (BCFAs) in men with benign prostatic hyperplasia (BPH) and metabolic syndrome (MetS), *Aging*, 2021, **13**(8), 10934–10954.

35 H. Chen, J. Qin and Y. Hu, Efficient degradation of high-molecular-weight hyaluronic acid by a combination of ultrasound, hydrogen peroxide, and copper ion, *Molecules*, 2019, **24**(3), 617.

36 S. Chen, H. Chen, R. Gao, *et al.*, Degradation of hyaluronic acid derived from tilapia eyeballs by a combinatorial method of microwave, hydrogen peroxide, and ascorbic acid, *Polym. Degrad. Stabil.*, 2015, **112**, 117–121.

37 H. Ye, X. Y. Liu and H. Hong, Characterization of sintered titanium/hydroxyapatite biocomposite using FTIR spectroscopy, *J. Mater. Sci.: Mater. Med.*, 2009, **20**, 843–850.

38 M. Tatzber, M. Stemmer, H. Spiegel, *et al.*, FTIR-spectroscopic characterization of humic acids and humin fractions obtained by advanced NaOH, $Na_4P_2O_7$, and Na_2CO_3 extraction procedures, *J. Plant Nutr. Soil Sci.*, 2007, **170**(4), 522–529.

39 I. Rehman and W. J. J. Bonfield, Characterization of hydroxyapatite and carbonated apatite by photo acoustic FTIR spectroscopy, *J. Mater. Sci.: Mater. Med.*, 1997, **8**(1), 1–4.

40 D. W. Tao, Y. Qin, G. Huan, *et al.*, Dynamic changes of structural characteristics of snow chrysanthemum polysaccharides during *in vitro* digestion and fecal fermentation and related impacts on gut microbiota, *Food Res. Int.*, 2020, **141**(prepublish), 109888.

41 X. Bing, S. Shiqing, Y. Lingyun, *et al.*, Digestion under saliva, simulated gastric and small intestinal conditions and fermentation *in vitro* by human gut microbiota of polysaccharides from *Ficus carica* Linn, *Food Hydrocolloids*, 2024, **146**, 109204.

42 S. Şahinkaya, COD and color removal from synthetic textile wastewater by ultrasound assisted electro-Fenton oxidation process, *J. Ind. Eng. Chem.*, 2013, **19**(2), 601–605.

43 L. Xu, X. Zhang, J. Han, *et al.*, Degradation of emerging contaminants by sono-Fenton process with *in situ*

generated H_2O_2 and the improvement by P25-mediated visible light irradiation, *J. Hazard. Mater.*, 2020, **391**, 122229.

44 Y. M. Go and D. P. Jones, Thiol/disulfide redox states in signaling and sensing, *Crit. Rev. Biochem. Mol. Biol.*, 2013, **48**(2), 173–181.

45 C. H. Johnson, J. Ivanisevic and G. Siuzdak, Metabolomics: beyond biomarkers and towards mechanisms, *Nat. Rev. Mol. Cell Biol.*, 2016, **17**(7), 451–459.

46 B. Mohammadali, D. Sylvain, V. Konstantin, *et al.*, Assessment of Membrane and Electrochemical Technologies for the Treatment of a Selenium-Bearing Mine water: Technology Performance and Effect on Toxicity and Bioaccumulation, *Mine Water Environ.*, 2023, **42**(3), 361–382.

47 V. W. Oliveira, F. C. M. Silva, R. B. Araújo, *et al.*, Assessment of homogeneous electro-Fenton process coupled with microbial fuel cell utilizing *Serratia* sp. AC-11 for glyphosate degradation in aqueous phase, *J. Environ. Manage.*, 2024, **370**, 122797.

48 K. Qin, F. Wang, R. M. L. Simpson, *et al.*, Hyaluronan promotes the regeneration of vascular smooth muscle with potent contractile function in rapidly biodegradable vascular grafts, *Biomaterials*, 2020, **257**, 120226.

49 H. Sies, C. Berndt and D. P. Jones, Oxidative stress, *Annu. Rev. Biochem.*, 2017, **86**(1), 715–748.

50 C. W. Lee, J. Y. Seo, J. W. Choi, *et al.*, Potential anti-osteoporotic activity of low-molecular weight hyaluronan by attenuation of osteoclast cell differentiation and function in vitro, *Biochem. Biophys. Res. Commun.*, 2014, **449**(4), 438–443.

51 M. F. Neurath, Targeting immune cell circuits and trafficking in inflammatory bowel disease, *Nat. Immunol.*, 2019, **20**(8), 970–979.

52 J. Wang, Q. Zhang, Z. Zhang, *et al.*, International journal of biological macromolecules, *Int. J. Biol. Macromol.*, 2024, **280**, 135553.

53 L. Chevolot, A. Foucault, F. Chaubet, *et al.*, Further data on the structure of brown seaweed fucans: relationships with anticoagulant activity, *Carbohydr. Res.*, 1999, **319**(1–4), 154–165.

54 G. Ruichang, C. Hui, L. Laihao, *et al.*, Preparation and antioxidant properties of low molecular weight hyaluronic acid from tilapia eyes, *Sci. Technol. Food Ind.*, 2015, (03), 60–64.

55 Y. Qi, L. Wang, Y. You, *et al.*, Preparation of low-molecular-weight fucoidan with anticoagulant activity by photocatalytic degradation method, *Foods*, 2022, **11**(6), 822.

56 L. Chevolot, A. Foucault, F. Chaubet, *et al.*, Further data on the structure of brown seaweed fucans: relationships with anticoagulant activity, *Carbohydr. Res.*, 1999, **319**(1–4), 154–165.